Chemical Geology 304-305 (2012) 39–52

Contents lists available at SciVerse ScienceDirect

Chemical Geology

journal homepage: www.elsevier.com/locate/chemgeo

Research papers

Mapping $^{87}Sr/^{86}Sr$ variations in bedrock and water for large scale provenance studies

Clément P. Bataille *, Gabriel J. Bowen

Department of Earth and Atmospheric Sciences, Purdue University, West Lafayette, Indiana 47907, USA

ARTICLE INFO

Article history:
Received 1 June 2011
Received in revised form 23 January 2012
Accepted 24 January 2012
Available online 31 January 2012

Editor: J.D. Blum

Keywords:
Strontium rubidium method
Isoscape
GIS
Strontium isotope ratio
Provenance

ABSTRACT

Although variation in $^{87}Sr/^{86}Sr$ has been widely pursued as a tracer of provenance in environmental studies, forensics, archeology and food traceability, accurate methods for mapping variations in environmental $^{87}Sr/^{86}Sr$ at regional scale are not available. In this paper, we build upon earlier efforts to model $^{87}Sr/^{86}Sr$ in bedrock by developing GIS-based models for Sr isotopes in rock and water that include the combined effects of lithology and time. Using published data, we fit lithology-specific model parameters for generalized equations describing the concentration of radiogenic Sr in silicate and carbonate rocks. The new model explained more than 50% of the observed variance in measured Sr isotope values from independent global databases of igneous, metaigneous, and carbonate rocks, but performed more poorly (explaining 33% of the variance) for sedimentary and metasedimentary rocks. In comparison, a previously applied model formulation that did not include lithology-specific parameters explained only 20% and 8% of the observed variance for igneous and sedimentary rocks, respectively, and exhibited an inverse relationship with measured carbonate rock values. Building upon the bedrock model, we also developed and applied equations to predict the contribution of different rock types to $^{87}Sr/^{86}Sr$ variations in water as a function of their weathering rates and strontium content. The resulting water model was compared to data from 68 catchments and shown to give more accurate predictions of stream water $^{87}Sr/^{86}Sr$ ($R^2 = 0.70$) than models that did not include lithological weathering parameters. We applied these models to produce maps ("isoscapes") predicting $^{87}Sr/^{86}Sr$ in bedrock and water across the contiguous USA, and compared the mapped Sr isotope distributions to data on Sr isotope ratios of US marijuana crops. Although the maps produced here are demonstrably imperfect and leave significant scope for further refinement, they provide an enhanced framework for lithology-based Sr isotope modeling and offer a baseline for provenance studies by constraining the $^{87}Sr/^{86}Sr$ in strontium sources at regional scales.

1. Introduction

Strontium isotope ratio measurements ($^{87}Sr/^{86}Sr$) have been applied in a wide variety of geoscience studies including chronostatigraphy of marine sediments (Veizer et al., 1999), petrology of igneous rocks (DePaolo, 1981), cation provenance and mobility (Chaudhuri and Clauer, 1993; Miller et al., 1993; Grousset and Biscaye, 2005; Chadwick et al., 2009), and quantitative models of chemical weathering (Clow et al., 1997; Horton et al., 1999). More recently the use of $^{87}Sr/^{86}Sr$ has been extended to a wide range of new applications in hydrology (Hogan et al., 2000), forensics (Beard and Johnson, 2000; West et al., 2009), archeology (Hodell et al., 2004; Bentley et al., 2008), ecology (Koch et al., 1995; Chamberlain et al., 1997; Hoppe et al., 1999; Barnett-Johnson et al., 2008) and food traceability (Kelly et al., 2005; Crittenden et al., 2007; Voerkelius et al., 2010). These applications are based on the principle that $^{87}Sr/^{86}Sr$ of natural materials reflects the sources of strontium (Sr) available during their formation (Dasch, 1969). For instance, in studies of animal provenance, the $^{87}Sr/^{86}Sr$ of the Sr assimilated in animal tissues reflects the different sources of ingested Sr obtained from water and/or food (Graustein, 1989). As a consequence, variations in $^{87}Sr/^{86}Sr$ of these tissues can be used to trace migration or changes in diet habits of a given organism (Capo et al., 1998). Interpreting the $^{87}Sr/^{86}Sr$ signature for provenance studies requires constraining the $^{87}Sr/^{86}Sr$ variations of potential environmental sources of Sr. In this work, we attempt to model the spatial variations of $^{87}Sr/^{86}Sr$ in bedrock and water, two important sources of Sr to biological systems.

The use of $^{87}Sr/^{86}Sr$ as a tracer is of particular interest because unlike for isotopes of the light elements, biological and instrumental mass-dependent fractionations are automatically corrected during measurements and thus, the $^{87}Sr/^{86}Sr$ directly reflects the Sr of the source. In addition their wide amplitude of variation on both large and small scales, low temporal variability, and relative high abundance for a trace element make Sr isotopes a strong candidate for tracing inorganic and organic materials, either independently or in conjunction with isotopic data from lighter elements (Graustein and Armstrong, 1983; Kawasaki et al., 2002; Bowen et al., 2005; Bowen, 2010).

* Corresponding author. Tel.: +1 765 404 4772; fax: +1 765 496 1210.
E-mail address: cbataill@purdue.edu (C.P. Bataille).

0009-2541/$ – see front matter © 2012 Elsevier B.V. All rights reserved.
doi:10.1016/j.chemgeo.2012.01.028

Several different approaches have been taken to map Sr isotopic variations at large scale. The fundamental theory underlying Sr isotope variation in geological material was summarized by Faure (1977), who proposed two equations describing the evolution of $^{87}Sr/^{86}Sr$ in mantle and crustal rocks that remain the basis for modeling $^{87}Sr/^{86}Sr$ in bedrock. Although several efforts were made to map $^{87}Sr/^{86}Sr$ available to ecosystems over local to regional scales based on field measurements in water, soils and organisms (Price et al., 1994; Ezzo et al., 1997; Hodell et al., 2004; Bentley and Knipper, 2005), Beard and Johnson (2000) made the first attempt to model $^{87}Sr/^{86}Sr$ variations in bedrock over large spatial scales. In their work, Beard and Johnson simplified Faure's theory by considering rock age to be the only determinant of $^{87}Sr/^{86}Sr$ variations and mapped the $^{87}Sr/^{86}Sr$ in the USA based on rock unit ages reported in a digital geological map. Their study suggested strongly patterned $^{87}Sr/^{86}Sr$ variations at continental scales but did not include systematic verification from field measurements. Nor did the authors advocate the use of their 'fist-pass' model for quantitative prediction of Sr isotope ratios. Because bedrock weathering is the ultimate source of Sr to biological systems, however, these authors proposed that with improved understanding the modeled patterns could be used to interpret the geographic origin of biological materials.

Although bedrock Sr is the ultimate source of Sr to Earth surface systems, its isotopic composition can differ substantially from that of soils, surface water and organisms due to factors such as variation in weathering rates for different minerals or inputs from other sources such as atmospheric aerosols (Capo et al., 1998; Stewart et al., 1998; Bentley, 2006; Chadwick et al., 2009). For constraining the isotopic variations in source of Sr for provenance studies it is most appropriate to model the "biologically available Sr" as an approximation of the Sr actually assimilated by organisms (Sillen et al., 1998; Price et al., 2002; Hodell et al., 2004; Frei and Frei, 2011). In this regard, a theoretical steady state and time dependent model predicting $^{87}Sr/^{86}Sr$ evolution in "biologically available Sr" has been developed (Stewart et al., 1998). This model details the potential factors and sources causing transfers of Sr from soil to water and from water to ecosystems, but its applicability remains limited at regional scale because of the large number of variables to be constrained. Furthermore, this model relies on empirical measurements to obtain the $^{87}Sr/^{86}Sr$ variations in bedrock (Stewart et al., 1998).

An alternative approach to mapping spatial Sr isotope variation has been proposed by the TRACE project, which developed an empirical model for predicting $^{87}Sr/^{86}Sr$ in groundwater based on the measurement of 650 different European natural mineral waters (Voerkelius et al., 2010). Using this dataset and a geological map of Europe, a mean $^{87}Sr/^{86}Sr$ was calculated for each geological unit underlying sampled waters, and these values were extrapolated to similar rock units to develop a comprehensive prediction map for the continent. Although this model was shown to reproduce the large scale patterns of $^{87}Sr/^{86}Sr$ variations in biological materials, it requires iterative subjective analysis of regional geological and Sr isotope data and as a result is not immediately generalizable to other regions. Furthermore, the prediction accuracy of this approach is highly dependent on the density of sampling, and improving the resolution or extending the spatial coverage will require expensive field campaigns.

These previous efforts illustrate the difficulties of mapping $^{87}Sr/^{86}Sr$ variation at different scales in different sources. In this paper, we focus on developing scalable spatial $^{87}Sr/^{86}Sr$ predictions for bedrock and water. We build upon the effort of Beard and Johnson to map $^{87}Sr/^{86}Sr$ in bedrock and we developed a simplified model of Sr cycling (Stewart et al., 1998) to extend $^{87}Sr/^{86}Sr$ prediction to water and ecosystems. We validate the models by using existing $^{87}Sr/^{86}Sr$ measurements. The resulting models provide baseline predictions for rock and water $^{87}Sr/^{86}Sr$ across the contiguous USA, and can be used over a range of spatial resolutions depending on the application of interest. Although these models are demonstrably imperfect and incomplete and their predictive power limited with respect to that desired in many potential applications, this work represents an important step towards developing systematic spatial predictions for Sr isotopes with wide geochemical applications.

2. Bedrock models

Model derivation, calibration, and validation are described in the following sections. Additional details and documentation are available in the accompanying Supplementary material.

2.1. Silicate model theory

^{87}Sr production in rocks results from the radioactive decay of ^{87}Rb, which decays to ^{87}Sr with a half-life of 49 billion years. In a closed system, the ratio of radiogenic ^{87}Sr to the stable isotope ^{86}Sr in rocks slowly increases with time (t) as a function of the rock's Rb/Sr ratio:

$$\frac{^{87}Sr}{^{86}Sr} = \left(\frac{^{87}Sr}{^{86}Sr}\right)_i + \frac{Rb}{Sr}\left(e^{\lambda t} - 1\right), \quad (1)$$

where λ is the decay constant of the parent isotope ($1.42 * 10^{-11}\ yr^{-1}$) and $(^{87}Sr/^{86}Sr)_i$ is the initial $^{87}Sr/^{86}Sr$ (Faure, 1977). Rb/Sr varies between different layers and different rocks because geochemical processes fractionate Rb and Sr due to the specific affinity of each element for different minerals (Carlson, 2003). Rb substitutes better for potassium (K) and Sr for calcium (Ca) in minerals, and Rb/Sr tends to be high in felsic and K-bearing sedimentary rocks and low in mafic and carbonate rocks (Rudnick, 2003). The dissimilar affinities of Rb and Sr cause Rb/Sr to vary at large scales between the mantle and the crust and at small scales between different rocks and minerals (Rudnick, 2003).

Our model attempts to trace the evolution of $^{87}Sr/^{86}Sr$ values in silicate rocks from the time of Earth's formation to present (Fig. 1). We consider that the geological history of each rock started 4.5 billion years ago in a chemically homogeneous Earth. At that time, the Rb and Sr present in the earth were well-mixed and the $^{87}Sr/^{86}Sr$ is estimated to have been 0.699 based on measurements of chondrites (Wasserbu et al., 1969). Prior to crustal differentiation, the $^{87}Sr/^{86}Sr$ evolved slowly but homogeneously in the bulk earth. Following differentiation, different crustal layers inherited a higher Rb/Sr than the mantle due to the higher affinity of Rb for crustal minerals. Consequently, as the crust evolved, its $^{87}Sr/^{86}Sr$ deviated from the residual mantle value (Faure, 1977). As new rocks were formed from crustal

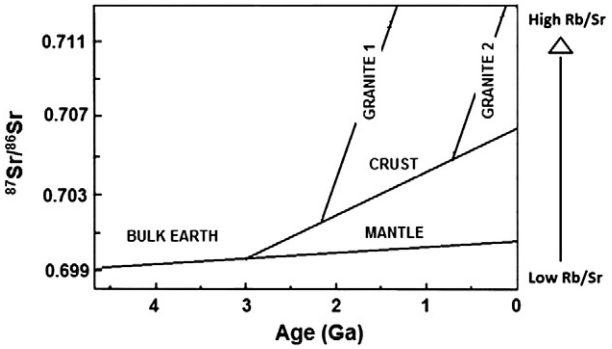

Fig. 1. Three-stage model for the evolution of $^{87}Sr/^{86}Sr$ in Earth materials through geological time. ^{87}Sr accumulates in all pools due to ^{87}Rb decay, with the rate depending of the Rb/Sr of each lithology. Granite1 and Granite2 are examples of rock formation occurring at different time during earth history. Modified from Encyclopedia of Geochemistry (2000) and Capo et al. (1998).

or mantle precursors, they inherited the $(^{87}Sr/^{86}Sr)_i$ of their parent, but in most cases had different Rb/Sr, causing their $^{87}Sr/^{86}Sr$ to evolve along a different Rb/Sr slope than the parent material. Rocks with higher (lower) Rb/Sr than their parent evolved along a steeper (flatter) slope.

Because Rb and Sr are fractionated differently in geological processes, the Rb/Sr of a rock can be modified during tectonic, metamorphic or sedimentary transformations, thus modifying the $(^{87}Sr/^{86}Sr)_i$ or the slope of evolution of $^{87}Sr/^{86}Sr$. For example, $(^{87}Sr/^{86}Sr)$ and Rb/Sr values for the Idaho batholiths have been shown to vary largely along a 700 m transect depending on what host rock the batholith intruded (King et al., 2007). Since most geological materials in the crust have been recycled multiple times throughout earth history, and this history of transformations is usually incompletely documented in geological map data, the comprehensive history of $^{87}Sr/^{86}Sr$ evolution is difficult to reconstruct.

In our model, we make the simplifying assumption that the modern $^{87}Sr/^{86}Sr$ of silicate rocks can be approximated based on a three stage history, where all rocks of a given lithology are assumed to have been derived from a common parent material. In each new stage, it is assumed that the new rock produced inherits its parent material's mean $^{87}Sr/^{86}Sr$, but is differentiated chemically (Rb/Sr) from the parent material. First, ^{87}Sr was produced in the chemically undifferentiated Earth until an $^{87}Sr/^{86}Sr$ of 0.701 was reached at 3 Ga. At 3 Ga (an approximation of the age of crustal differentiation, t_1) chemical differentiation occurred, and from that time $^{87}Sr/^{86}Sr$ evolved independently in the mantle and multiple crustal rock reservoirs. Extant rock units were formed from one of these rock reservoirs at times corresponding to their ages (t_2) as documented in geological map data.

This theoretical framework gives:

$$\left(\frac{^{87}Sr}{^{86}Sr}\right)_{rock} = 0.701 + \left(\frac{Rb}{Sr}\right)_{parent}\left(e^{\lambda(t_1-t_2)}-1\right) + \left(\frac{Rb}{Sr}\right)_{rock}\left(e^{\lambda t_2}-1\right), \quad (2)$$

where $(Rb/Sr)_{parent}$ is the Rb/Sr of the parent material, and $(Rb/Sr)_{rock}$ is the Rb/Sr of the modern rock.

2.2. Silicate model calibration

Calculating the $^{87}Sr/^{86}Sr$ of a rock unit using Eq. (2) requires estimates of the parameters $(Rb/Sr)_{parent}$ and $(Rb/Sr)_{rock}$ as well as the approximate age the rock. Information on rock age is a common feature of digital geological maps, but estimating the parameters $(Rb/Sr)_{parent}$ and $(Rb/Sr)_{rock}$ for each lithology is not as straight forward. We proceeded in two steps by calibrating the silicate model independently for each parameter.

In the first calibration step, we assigned values for $(Rb/Sr)_{parent}$, which determines the slope of $^{87}Sr/^{86}Sr$ evolution during stage 2. This parameter depends on the type of parent material (Fig. 1) which includes: 1) weathered bedrock for sedimentary material, 2) magma for igneous rock, 3) the parent lithology for metamorphic rocks. In the absence of information concerning the parent rock, we approximated the $(Rb/Sr)_{parent}$ of sedimentary and metasedimentary rocks by assuming that they originate from a uniform source with a constant value of 0.24 corresponding to the average Rb/Sr of the upper crust (Goldstein and Jacobsen, 1988). To approximate the $(Rb/Sr)_{parent}$ of igneous and metaigneous rocks, we separated these lithologies in 5 categories (ultramafic, mafic, intermediate, felsic intermediate and felsic) using the International Union of Geological Sciences (IUGS) classification (Le Bas and Streckeisen, 1991). This effectively separates igneous rocks between Rb-poor mantle rocks and Rb-rich crustal rocks. We used data from the Western North American Volcanic and Intrusive Rock Database (www.navdat.org), including measurements for $(^{87}Sr/^{86}Sr)_{rock}$, age (t_2) and $(Rb/Sr)_{rock}$), to back-calculate the $(Rb/Sr)_{parent}$ for each of 5765 samples using Eq. (2). Finally, we classified these samples according to our 5 categories and calculated the average $(Rb/Sr)_{parent}$ for samples in each category (see Supplementary Table 1).

In the second calibration step, we assigned values to the parameter $(Rb/Sr)_{rock}$ by estimating the average Rb/Sr for 180 silicate rock unit types appearing in the United States Geological Survey state-level geological map geodatabases (Geological Survey (U.S). State Geologic Map Compilation, 2005). For each of these rock unit types, we calculated the average (Rb/Sr) from identical or analogous lithologies in the USGS geochemical database (Geological Survey (U.S.) The National Geochemical Survey, 2004). We used this database because it included a large number of Rb and Sr measurements (252,661 measurements) covering 167 of the 180 lithologies selected. The 13 remaining lithologies were assigned $(Rb/Sr)_{rock}$ by comparison with other analogous rocks (see Supplementary Table 1).

2.3. Carbonate model calibration

We modeled carbonate rocks separately because their $(^{87}Sr/^{86}Sr)_i$ is not dependent on decay, but is a function of the variations of $^{87}Sr/^{86}Sr$ in seawater:

$$\left(\frac{^{87}Sr}{^{86}Sr}\right)_{rock} = \left(\frac{^{87}Sr}{^{86}Sr}\right)_{seawater} + \left(\frac{Rb}{Sr}\right)_{rock}\left(e^{\lambda t_2}-1\right). \quad (3)$$

We apply the carbonate model to 10 lithologies from the USGS state-level geological map geodatabase (Supplementary material Table 1). Values of $(^{87}Sr/^{86}Sr)_{seawater}$ were estimated for each rock age (Supplementary Table 2) using $^{87}Sr/^{86}Sr_{seawater}$ curves from the Precambrian Marine Carbonate Isotope Database (PMCI) (Shields and Veizer, 2002; see Supplementary Table 3). The estimation of $(Rb/Sr)_{rock}$ values for each carbonate lithology was conducted as described for silicates in Section 2.2 (see Supplementary Table 1).

2.4. Model validation

We conducted separate validation exercises for igneous and sedimentary rocks because of the difference in calibration methods for $(Rb/Sr)_{parent}$ described in Section 2.2. We expect a lower accuracy of the silicate model for sedimentary rock due to the absence of information concerning the parent rock for this type of rock. We used 9130 igneous rock and 207 sedimentary rock data from the global GEOROC database (Lehnert et al., 2000). The parameterized silicate model was applied to independently predict the $^{87}Sr/^{86}Sr$ of samples represented in these databases using the parameter values from Supplementary Table 1 associated with the database-specified lithology, and the predicted and observed values were compared. Data from 121 samples (1.3% of the samples) were removed from the igneous rock validation dataset. Among these samples, 78 (0.85% of all samples) were old felsic rocks (granites or rhyolites) displaying exceptionally high $^{87}Sr/^{86}Sr$ ranging from 0.850 to 4. These samples are also characterized by unusually high Rb/Sr ranging from 744 to 30. We recognize as a limitation of the current version of our model that it cannot accurately account for such highly radiogenic samples. The remaining 43 samples (0.47% of all samples) corresponded to rocks displaying $^{87}Sr/^{86}Sr$ values that are highly atypical for their lithological classification: e.g., 6 basalts were removed because their $^{87}Sr/^{86}Sr$ was higher than 0.730. In these cases we suspect that the database classifications provided an inaccurate or incomplete description of the sample lithology.

We validated the carbonate model by comparing model predictions with 246 published data from the PMCI (Shields and Veizer, 2002) and the GEOROC database (Lehnert et al., 2000). Although this comparison does not represent a completely independent validation of the model since some of the validation data were used in

reconstructing the paleo-seawater Sr isotope curves, it allows us to provide a first order assessment of model performance.

Although the validation data used here provide a broad representation of lithologies and ages they are not comprehensive, and thus limit our ability to validate the model, in that: 1) analyses gathered in these databases are biased toward rocks from active tectonic and volcanic areas, 2) $^{87}Sr/^{86}Sr$ values for continental sedimentary samples are under-represented in comparison with igneous rocks, and 3) Mesozoic and Cenozoic rocks represent more than 80% of the samples in the database. Additional inaccuracies in our parameterization and validation could result from a lack of control on the degree of alteration of database samples, which could lead to: 1) overestimation of Rb/Sr values because Sr is preferentially removed during weathering (Dasch, 1969), or 2) underestimation of $^{87}Sr/^{86}Sr$ values because rock preferentially lose Sr from their low $^{87}Sr/^{86}Sr$ mineral phases during weathering (e.g. Bullen et al., 1996).

2.5. Mapping bedrock $^{87}Sr/^{86}Sr$

Using the above equations, we calculated Sr isotope ratios for 319,824 mapped geological units represented in the United States Geological Survey state-level geological map geodatabases (Geological Survey (U.S). State Geologic Map Compilation, 2005). Although these maps present some challenges (see Supplementary methods and http://pubs.usgs.gov/of/2005/1325/documents/CONUSdocumentation.pdf), they are unique in providing internally consistent, high resolution age and lithological information for the contiguous USA.

The 48 state lithological maps of the conterminous USA were downloaded in shape file format. Using ArcGIS, we merged the individual maps into a single shape file to obtain a geodatabase with three attributes relevant to our work:

- Unit_age: the text descriptor of the maximum age of the unit, and
- Rocktype1, and Rocktype2: the major and minor lithology descriptors.

We used these fields to join the map unit table with a set of tables containing the parameter values used in Eqs. (2) and (3):

- The table "Age" (Supplementary Table 2) listed each unique geologic time descriptor found in the map units table and related the attribute MAXAGE with a numeric age estimated from the USGS geological time scale (Geological Survey (U.S.). Geologic Names Committee, 2007).
- The tables "Lithology1" and "Lithology2" listed each lithologic descriptor present in the geodatabase and assigned values for the parameters $(Rb/Sr)_{parent}$ and $(Rb/Sr)_{lithology}$ (Supplementary Table 1).
- The table "Carbonates" (Supplementary Table 3) associated carbonate rock age with the $^{87}Sr/^{86}Sr$ of seawater.

Using the values from these associated tables, we calculated $^{87}Sr/^{86}Sr$ for each map polygon (geological map unit). In cases where both major and minor lithologies were documented for a map unit, we calculated separate Sr isotope ratio estimates for each lithology.

3. Water models

3.1. Theory

The $^{87}Sr/^{86}Sr$ of soluble Sr in stream water is largely determined by the delivery of Sr to runoff by chemical weathering of the underlying bedrock (Stewart et al., 1998), though in some cases the soluble Sr in water can originate from other inputs such as groundwater (Négrel and Petelet-Giraud, 2005) atmospheric deposition of sea salt and mineral dust (Chadwick et al., 2009), hydrothermal processes (Pretti and Stewart, 2002), or soils and surficial deposits (Stueber et al., 1975). Chemical weathering of bedrock is regulated by a complex combination of factors including lithological and mineralogical composition (Meybeck, 1987; Horton et al., 1999; Brantley et al., 2007), climate (particularly temperature and runoff; White and Blum, 1995), biology (Eckhardt, 1979; Brady and Carroll, 1994; Moulton et al., 2000) and erosion rates (Raymo et al., 1988; West et al., 2005). While these factors may be important for local studies, lithology and runoff have been identified as the two main controls of chemical weathering rates at regional scale (Beusen et al., 2009; Hartmann et al., 2009a; Jansen et al., 2010; Hartmann and Moosdorf, 2011). In order to simplify our large scale model, we limited our analysis to a pair of first order lithologically-based factors influencing the flux of Sr to water: 1) differential weathering rates of rocks and minerals, which we represent as a dimensionless weathering rate factor W (Supplementary Table 4), and 2) differences in Sr content (C) between lithologies. The chemical weathering of carbonates versus silicates illustrates the importance of these factors: carbonates have a higher Sr content and weather faster than silicates, therefore even trace quantities of calcite can be a dominant source of soluble Sr and control the $^{87}Sr/^{86}Sr$ of environmental waters (Clow et al., 1997; Anderson et al., 2000).

3.2. Weathering model calibration

In our model, the transfer of Sr from a rock to water is given by:

$$F = W_{norm}C, \tag{4}$$

where F is the flux of Sr from rock to water, C is the average Sr content (Supplementary Table 4) of each rock type calculated as described for Rb/Sr_{rock} in Section 2.2 and W_{norm} is the weathering rate normalized to granite (Supplementary Table 4). We adopted two different approaches to estimating W_{norm}, depending on rock type. To estimate W_{norm} for igneous and sedimentary rocks, we calculated bulk rock dissolution rates for each rock type as:

$$K_{rock} = \sum_i a_i K_i, \tag{5}$$

where i is a given mineral, a_i is abundance of i in the given rock type and K the weathering rate value for that mineral based on laboratory measurements. We estimated a_i from the IUGS classification (Le Bas and Streckeisen, 1991; Supplementary Table 4). Mineral-specific values of K were taken from averaged values of mineral weathering rates found in laboratory experiments at pH = 5.5 and T = 20 °C (Supplementary Table 5; Franke, 2009). However, because field studies suggest that at equal mineralogical composition, relative weathering rates of igneous and volcanic rocks differs (Drever and Clow, 1995), we scaled our W estimate as:

$$W_{norm} = \frac{K_{rock}R}{K_{granite}}, \tag{6}$$

where R is a correction factor related to differential reactive surface between rock type. Values of R were assigned by grouping rock types into three broad categories chosen to account for differences in permeability, and thus reactivity with aqueous solutions (Lewis, 1989), and comparing our calculated values of W_{norm} for each category with dissolution rate measurements in small monolithic catchments in France (Meybeck, 1987; Meybeck, 1987). The assigned values (R = 3 for volcanic rocks, R = 2 for metavolcanic and R = 1 for crystalline igneous rocks) offer a rough approximation of relative field weathering rates useful for our initial large scale effort, and can be refined in future work.

Because the mineralogy of metamorphic and sedimentary rocks is difficult to estimate, we estimated W_{norm} of silicate sedimentary, pyroclastic and metamorphic rocks using a different approach. Based

on denudation rate measurements from small monolithic catchments (Meybeck, 1987; Meybeck, 1987), we distinguished between metamorphic and silicate sedimentary rocks, with low weathering rates similar to those of granite (assigned $W_{norm}=1$) and faster-weathering argillaceous sedimentary rocks ($W_{norm}=2$). Because no monolithic catchment dissolution rates measurements were available for pyroclastic rocks, we estimated W_{norm} from long term dissolution measurements of tuff tablets relative to those of granodiorite tablets exposed to the same conditions (Matsukura et al., 2007). Compared to regional scale estimates of chemical weathering based on dissolved silicate content (Bluth and Kump, 1994; Beusen et al., 2009; Hartmann et al., 2009; Jansen et al., 2010), our values show similar relative weathering rates across five major lithological groups: 1) carbonates and evaporites ($50>W_{norm}>25$), 2) tuff, pyroclastic flow and mafic volcanic rocks ($25>W_{norm}>5$), 3) other volcanic rocks and basic and intermediate igneous rocks ($5>W_{norm}>3$), 4) argilaceous sediments ($W_{norm}=2$) and 5) other metamorphic, sedimentary and felsic intrusive rock ($W_{norm}=1$). Although in good agreement with existing literature, our weathering formulation is limited in that it 1) does not account for runoff, climate, land cover or slope variations, and 2) is based on bulk dissolution rates and while accounting for differences in Sr content between rock type it does consider Sr-specific dissolution kinetics.

3.3. Mapping local and catchment water $^{87}Sr/^{86}Sr$

We combined the weathering and bedrock models to map $^{87}Sr/^{86}Sr$ variations in local and catchment-integrated waters. The local water model estimates the $^{87}Sr/^{86}Sr$ value of Sr leached from bedrock to water at each point on the map, whereas the catchment water model estimates the $^{87}Sr/^{86}Sr$ of surface waters flowing through each map location, including all contributions from up-catchment locations.

In the local water model, for each map unit polygon where major and minor lithologies were given we calculated the relative Sr weathering flux from major and minor lithologies:

$$(WC)_{tot} = 0.75*(WC)_{major} + 0.25*(WC)_{minor} \quad (7)$$

and the average Sr isotope ratio of local water, weighted by the fluxes from major and minor lithologies:

$$\left(\frac{^{87}Sr}{^{86}Sr}\right)_{local} = \left(\frac{0.75*(WC)_{major}}{(WC)_{tot}}\right)*\left(\frac{^{87}Sr}{^{86}Sr}\right)_{major} + \left(\frac{0.25*(WC)_{minor}}{(WC)_{tot}}\right)*\left(\frac{^{87}Sr}{^{86}Sr}\right)_{minor} \quad (8)$$

In these equations, the relative weights assigned to major and minor lithologies (0.75 and 0.25, respectively) represent a coarse generalization consistent with the only available constraint, that rocktype1 and rocktype2 are the most and second most abundant of the rock types present in each mapped unit (e.g. http://pubs.usgs.gov/of/2005/1325/documents/CONUSdocumentation.pdf).

Sr flux and local $^{87}Sr/^{86}Sr$ values were exported to raster data layers at 1 km spatial resolution for further analysis and mapping of catchment water $^{87}Sr/^{86}Sr$. The catchment water map was created using the Flow Accumulation tool (Spatial Analyst toolbox) in ArcGIS and 1 km gridded flow direction values from the Hydro 1 K digital elevation model (DEM; http://edc.usgs.gov/products/elevation/gtopo30/hydro/namerica.html). Modeled local water Sr isotope flux $[(^{87}Sr/^{86}Sr)_{local}\times(WC)_{tot}]$ and Sr flux $[(WC)_{tot}]$ values were accumulated downstream through the DEM river networks and divided to obtain estimated water $^{87}Sr/^{86}Sr$ values that represented an average of the up-stream Sr sources to each map pixel, weighted by the contribution of weathered Sr from each rock type in the catchment. We note that, although this model accounts for lithology-driven variation in weathered Sr fluxes, it does not explicitly calculate the water balance of the catchment and so does not account for differences in Sr flux driven by differences in runoff from individual grid cells.

3.4. Model validation

To validate the catchment water model, we compared $^{87}Sr/^{86}Sr$ predictions with water $^{87}Sr/^{86}Sr$ measured at 68 watersheds in 4 regions of the contiguous USA (Fig. 2). Before calculating $^{87}Sr/^{86}Sr$ in water, we obtained maps of the sub-watersheds for the Susquehanna River (http://www.srbc.net/atlas/index.asp) and the Owen Lake Basin (http://map24.epa.gov/EMR/). No pre-processed maps of the sub-watersheds existed for the Scioto River and Clark Fork of the Yellowstone River basins. Consequently, we delineated each catchment (Fig. 2) by processing the national elevation dataset (Gesch, 2002) with the Hydrology toolbox in ArcGIS (Spatial Analyst toolbox). We successively clipped the digital elevation model (DEM) for the area considered (Geoprocessing tool/Clip Raster), reconditioned the DEM (Fill Sinks tool), calculated the flow direction (Flow Direction tool) and flow accumulation (Flow Accumulation tool) rasters, defined streams by reclassifying the flow accumulation raster (Stream Definition tool; thresholds typically between 0.1 and 1% of the maximum flow accumulation), segmented the streams (Stream Segmentation tool) and finally delineated the watersheds and sub-watersheds (Watershed tool). We further validated this delineation process by comparing the shape of the catchments with the different maps furnished in published studies (Stueber et al., 1975; Fisher and Stueber, 1976; Horton et al., 1999; Pretti and Stewart, 2002).

In order to test the sensitivity of the catchment water model to different modeling assumptions, we used the Spatial Statistics tool (ArcGIS Spatial Analyst toolbox) to calculate three different estimates of the average $^{87}Sr/^{86}Sr$ for each catchment:

- Two estimates without weighting for differences in Sr flux among grid cells within the watershed. The first, which we call the "age-only catchment water model", is an unweighted average of $^{87}Sr/^{86}Sr$ values, calculated using the Beard and Johnson model (Beard and Johnson, 2000), across all grid cells in the catchment. The second, the "unweighted catchment water model" is an unweighted average of modeled "local water" $^{87}Sr/^{86}Sr$ values (Eq. 8) across all catchment grid cells.
- A third estimate accounted for differential Sr contributions from different map units within the catchment. This formulation, the "flux-weighted catchment water model", was equivalent to that used to map catchment water Sr isotope values as described above: the sum of the Sr isotope flux for all watershed grid cells was divided by the sum of the total Sr flux.

To further test the relevance of our models for provenance applications, we compared the $^{87}Sr/^{86}Sr$ predictions using these three formulations with the $^{87}Sr/^{86}Sr$ measured in marijuana from 79 USA counties (West et al., 2009). In this case, the samples were identified by their county of origin, and we averaged grid cell values within the county boundaries, as represented in the National Atlas of the United States (www.nationalatlas.gov/), rather than within catchments (Fig. 2).

4. Results and discussion

4.1. Bedrock model

The silicate model explained 59% of the observed variance in an independent global dataset for 9009 igneous and metamorphic rocks and 33% of the variance for 207 sedimentary rocks (Fig. 3A and B). This new silicate model significantly improved the correlation with measurements in comparison with estimates from the age-only

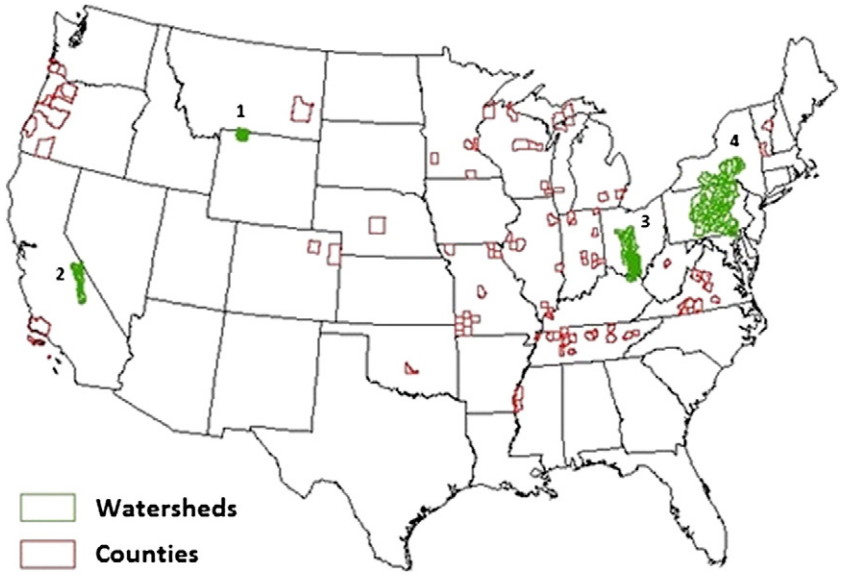

Fig. 2. Location of the samples used for the water model verification: Green: $^{87}Sr/^{86}Sr$ measurement in stream water from 1: Clarks Fork of the Yellowstone Basin (Horton et al., 1999); 2: Owens River Lake Basin (Pretti and Stewart, 2002); 3: Scioto River watershed (Stueber et al., 1975); 4: Susquehanna River Basin (Fisher and Stueber, 1976); Red: $^{87}Sr/^{86}Sr$ measurements of marijuana from 79 counties across the USA (West et al., 2009).

bedrock model. Moreover, for these datasets, the new model predictions cluster much closer to the 1:1 relationship than those of the age-only model. For the igneous and sedimentary datasets, respectively, the mean absolute error (MAE) of predictions are −0.00136 and −0.00968 for the silicate model and −0.00224 and −0.01936 for the age-only model. Whereas the age-only model globally underestimates the measured average $^{87}Sr/^{86}Sr$ (0.7059 and 0.7064 for the igneous and sedimentary data, respectively) and its variance ($7.95*10^{-6}$ and $3.07*10^{-6}$ respectively) in both datasets, the new silicate model predicts values for the average (0.7072 and 0.716 respectively) and variance (0.000134 and $6.46*10^{-5}$) of the validation datasets that are much closer to the observed values (average = 0.7082 and 0.7257, variance = 0.000348 and 0.000476). The root mean squared error for model predictions of igneous and sedimentary data in the validation datasets are 0.012 and 0.021 for the silicate model and 0.018 and 0.029 for the age-only model. In the absence of information about the parent rock, the first calibration step of the silicate model (Section 2.2) remains relatively inaccurate for sedimentary rocks, explaining the better performance of the model for igneous rocks than for sedimentary rocks. Overall, the new model has a tendency to underestimate $^{87}Sr/^{86}Sr$ values. These pattern likely results from the skewed distribution of samples in the calibration datasets (see Section 2.4). While this distribution is not representative of element distribution in nature (Reimann and Filzmoser, 2000) it leads during the calibration process to give best-fit parameter values that tend to underestimate $^{87}Sr/^{86}Sr$ values for rare, undersampled, highly radiogenic rocks.

The carbonates model, when validated against a dataset of 246 carbonate rocks (Shields and Veizer, 2002), explains more than half of the observed variance (Fig. 4). In contrast, the age-only model predictions are inversely correlated with observed $^{87}Sr/^{86}Sr$ in carbonates because they do not account for the very low (≈0) Rb/Sr of these rocks. As a result the age-only bedrock model over-predicts the Sr isotope ratios of ancient carbonates that formed at time when seawater $^{87}Sr/^{86}Sr$ was low.

The bedrock model performs much better on the igneous validation dataset when its predictions are compared with the mean values of the different lithologies (Fig. 5). This result reflects the fact that the parameterized model does not account for small-scale chemical variability within and between rock units of the same lithology that can have a substantial effects on Sr isotope ratios (see example Section 2.1 from King et al., 2007). Although the parameterized approach applied here does not allow accurate prediction of such small-scale $^{87}Sr/^{86}Sr$ variations within a rock unit, Fig. 5 shows that

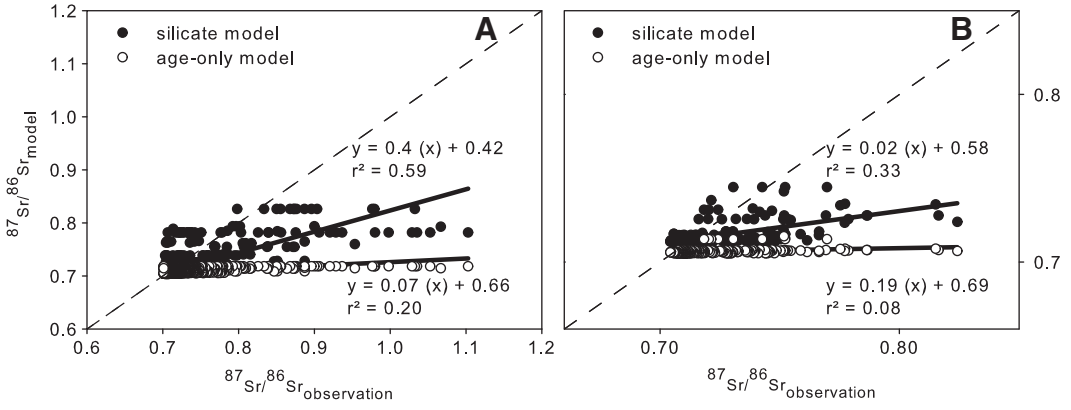

Fig. 3. Validation of silicate Sr isotope model. A. Linear correlation between 9009 worldwide $^{87}Sr/^{86}Sr$ igneous rock measurements and the $^{87}Sr/^{86}Sr$ predicted by the bedrock model and age-only model (Beard and Johnson, 2000). B. Linear correlation between 207 worldwide $^{87}Sr/^{86}Sr$ sedimentary rock measurements and the $^{87}Sr/^{86}Sr$ predicted by the bedrock model and age-only models. Dashed line in each panel shows the 1:1 relationship.

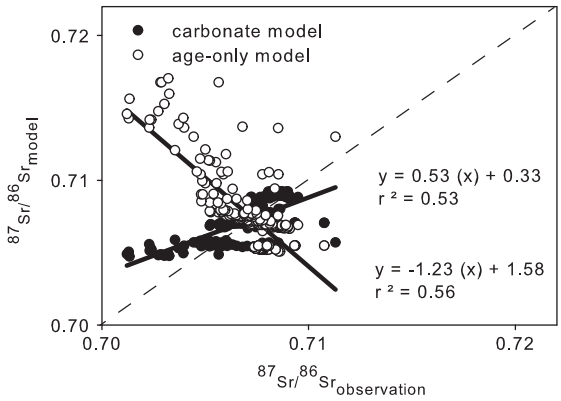

Fig. 4. Validation of carbonate Sr isotope model, showing linear correlations between 246 worldwide $^{87}Sr/^{86}Sr$measurements for carbonate rocks and the $^{87}Sr/^{86}Sr$ predicted by the bedrock model and age-only models. Dashed line shows the 1:1 relationship.

it does allow accurate predictions of the differences among lithologies within an independent validation dataset. Further improving the spatial resolution of the model will require coupling with models or data representing the evolution of magmatic fluids, metamorphic processes and sedimentary deposition at the scale of a rock unit.

Application of the bedrock model to predict Sr isotope ratios of major lithologies in rock units across the USA gives a range of predicted values from 0.704 to 0.816 (Fig. 6). The average $^{87}Sr/^{86}Sr$ for the USA is 0.7067 for the age-only model (Fig. 6B) and 0.7134 in the major bedrock model (Fig. 6A). Both models predict values below 0.716, the estimated average $^{87}Sr/^{86}Sr$ for the upper crust (Goldstein and Jacobsen, 1988). However, the major bedrock model more closely approaches this value and shows a much higher range of Sr isotope variations and higher maximum values for areas characterized by old rocks. Conversely, the age-only model more severely underestimates $^{87}Sr/^{86}Sr$ values and reduces the amplitude of variations relative to observations. Our results show that a large part of the inaccuracy found in the age-only model is driven by the omission of lithology-specific parameters.

In comparison with the age-only model, the major bedrock model shows more structure in $^{87}Sr/^{86}Sr$ variation over a range of spatial scales that are promising for provenance studies. On a continental scale (1000 km), we observe a general trend of decreasing $^{87}Sr/^{86}Sr$ from East to West. This trend is driven largely by the difference in rock age with older igneous rocks in the Appalachian and younger

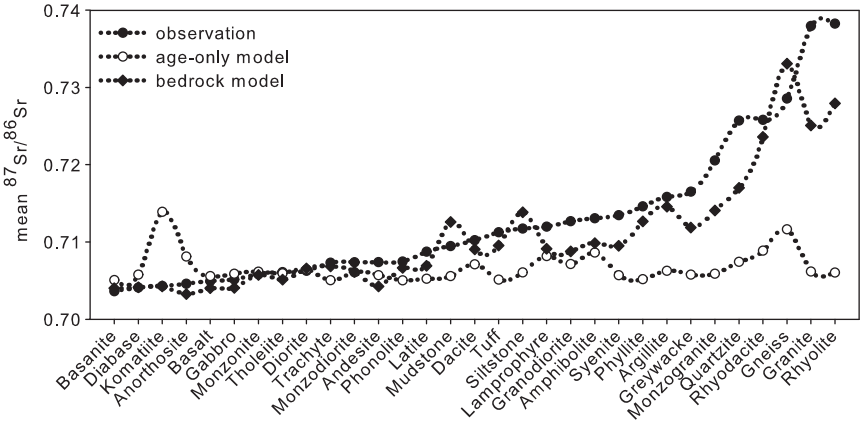

Fig. 5. Validation of silicate Sr isotope model by lithology. Average measured and predicted $^{87}Sr/^{86}Sr$ calculated for different lithologies represented in the global validation dataset. The dataset is the same as Fig. 3A but only lithologies with more than 10 available measurements have been selected.

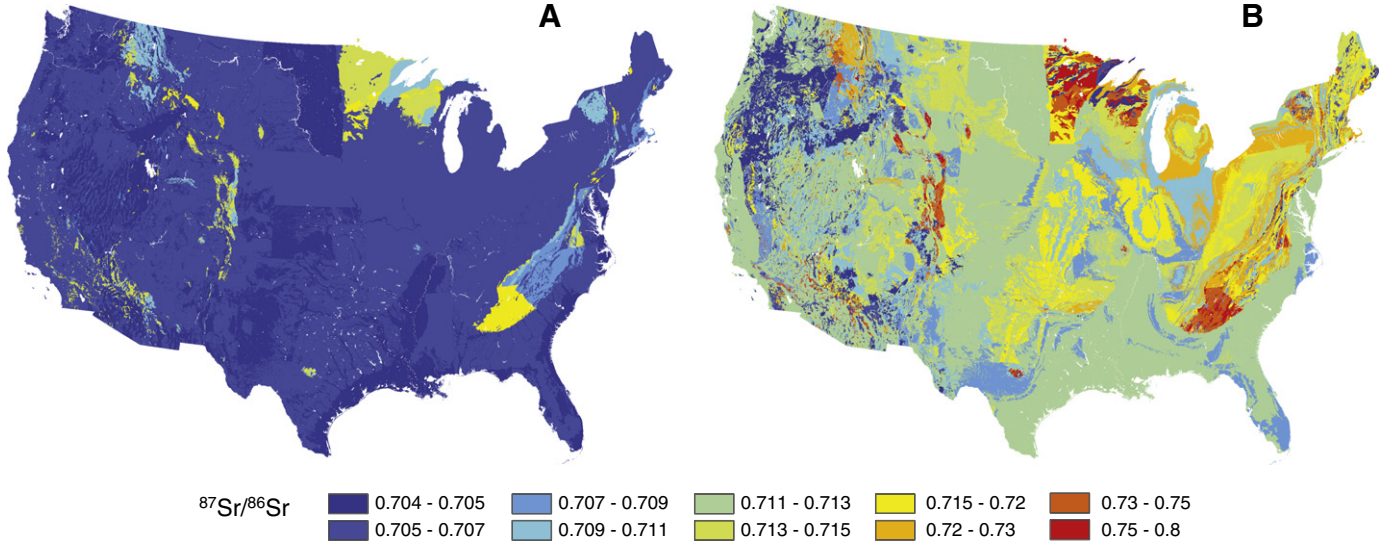

Fig. 6. Modeled bedrock Sr isotope ratios for the contiguous USA. A. Bedrock model $^{87}Sr/^{86}Sr$ variations in major bedrock lithologies for rock units throughout the USA, calculated using Eqs. (2) and (3); B. $^{87}Sr/^{86}Sr$ variations in the major bedrock using the age-only model (Beard and Johnson, 2000). $^{87}Sr/^{86}Sr$ discontinuities at state borders are related to inconsistencies in age or lithological classification between state geological maps and should be resolved through the development of a detailed, integrated, nation-wide map.

Table 1
Geology and measured and modeled $^{87}Sr/^{86}Sr$ values for bedrock in the catchment water model validation catchments. W: watershed; CF: Clark Fork of the Yellowstone; OL: Owen Lake; Sc: Scioto; Su: Susquehanna; N = North; S = South; E = East; W = West.

W	Geology	Sampled lithology	Measured $^{87}Sr/^{86}Sr$	Bedrock model $^{87}Sr/^{86}Sr$	Reference
CF	**N**: granitic gneiss Beartooth Mountains	Granitic gneiss	None	0.748	(Horton et al., 1999)
	S: Paleozoic marine sedimentary	Andesite		0.707	
	Eocene Andesite	Carbonates		0.7087	
OL	**W**: Sierra Nevada batholiths metavolcanic and igneous rocks	Sierra Nevada batholiths	0.706–0.725	0.706–0.722	(Goff et al., 1991)
	E: White–Inyo mountains complex mixture of sedimentary, igneous and metamorphic rocks (Marchand, 1974)	Volcanic rocks	0.706–0.708	0.707	(Goff et al., 1991)
		Tuff	0.709–0.713	0.711	(Davies and Halliday, 1998)
		Mesozoic granite	0.706–0.708	0.707	(Kistler and Peterman, 1973)
Sc	Mixture of Paleozoic shales and carbonates covered by glacial till	Devonian	0.7086	0.708–0.710	(Steele et al., 1972)
		Carbonates	0.732–0.745	0.719	
		Paleozoic shales	0.710		
		Shale leachate	0.708		
		Celestite			
Su	**N**: Mixture of silicates and carbonates from the Paleozoic	Shales	0.741–0.755	0.719	(Whitney and Hurley, 1964)
		Devonian limestone	0.7075	0.708–0.710	
	S: Precambrian to Mesozoic igneous, volcanic and metamorphic rocks	Igneous rocks	0.707–0.799	0.707–0.752	(Wetheril et al., 1968)

volcanic rocks in the West. On a regional scale (100 km), we observe large $^{87}Sr/^{86}Sr$ variations in sedimentary basins due to the difference between silicates and carbonates. High resolution $^{87}Sr/^{86}Sr$ variation is most apparent in mountainous areas due to the complex juxtaposition of lithologies in these regions. Even at the scale of a county (10 km), the bedrock models (major and minor) suggest the potential for high resolution $^{87}Sr/^{86}Sr$ variations depending on the lithological complexity.

4.2. Catchment water models

4.2.1. Water model validation

The four watersheds selected for model validation represent a wide range of geological, climatic and physiographic conditions (Fig. 2, Table 1). We compiled $^{87}Sr/^{86}Sr$ measurements from 68 streams in these watersheds: 1) 13 samples from the watershed of the Clarks Fork of the Yellowstone River (WY): a mountainous catchment with a predominant geology of granite, andesite and carbonates (Horton et al., 1999), 2) 19 samples from the Owens Lake watershed (CA): a mountainous watershed dominated by a complex mixture of igneous and metamorphic rocks associated with dolomite (Pretti and Stewart, 2002), 3) 19 samples from the Scioto River basin (OH): a sedimentary basin dominated by shales, sandstones and marine carbonates (Stueber et al., 1975), and 4) 18 measurements from the Susquehanna River basin (PA): a catchment containing varied sedimentary, metamorphic and igneous rocks (Fisher and Stueber, 1976). For each watershed the measured values reported in the literature were compared with three model estimates of the catchment-integrated average water Sr isotope ratio, as described in Section 3.4.

For each of these watersheds, because the bedrock models are the base maps of the catchment water model, we first tested the accuracy of the bedrock models by comparing the predictions with $^{87}Sr/^{86}Sr$ measurements of rock units within the selected watershed. Table 1 shows that for each of these watersheds, the bedrock model accurately predicts the $^{87}Sr/^{86}Sr$ of most lithologies, with the exception of the lower-than-predicted $^{87}Sr/^{86}Sr$ measured for shales from OH and PA and some igneous rocks from the Wissahickon formation (Owens Lake).

For the Clarks Fork of the Yellowstone Basin (Fig. 7A) each of the model formulations reproduces the basic pattern of $^{87}Sr/^{86}Sr$ differences across the sub-watersheds. However, the correlation (Fig. 7B) is closer to the 1:1 relationship for the flux-weighted catchment water model than for the unweighted and age-only catchment water models. In this basin, where Cenozoic sedimentary and volcanic rock coexists with Precambrian felsic rocks (Table 1), most of the $^{87}Sr/^{86}Sr$ variations in water are driven by the large differences in age of the different geological formations. In this geological setting, even if the age-only bedrock model does not account for differences in lithology it can be used to predict the first order patterns of variation in stream water $^{87}Sr/^{86}Sr$ values with reasonable accuracy. Prediction accuracy was further enhanced by incorporating lithological factors (Fig. 7B).

For the Owens Lake River Basin, in spite of the geological complexity of this watershed (Table 1), the $^{87}Sr/^{86}Sr$ of most streams was relatively constant at ~0.710 (Fig. 7C). In most of the streams, the flux-weighted catchment water model gives a more accurate prediction and stronger correlation (Fig. 7D) than the age-only and unweighted catchment water models. Silver Creek, located in the White–Inyo Mountains, is not correctly predicted by any of the water models. This stream runs through Cambrian marine sediments, gneisses and schists (Pretti and Stewart, 2002). In the catchment water models, the $^{87}Sr/^{86}Sr$ value is buffered to low values by the presence of dolomite with a predicted $^{87}Sr/^{86}Sr$ value of 0.709 (using our bedrock carbonate calculation). However, Pretti and Stewart (2002) argued that these dolomites probably exchanged Rb with shales during metamorphism and have significantly higher $^{87}Sr/^{86}Sr$ than otherwise expected, explaining the high $^{87}Sr/^{86}Sr$ in stream water of these catchments and the divergence with the modeled values.

McGee and Convict creeks, located in the Northern part of the Basin, lack metamorphosed dolomites in outcrop, but are also poorly predicted by the flux-weighted and unweighted catchment water models. These sub-watersheds present a complex hydro-geological setting, including Paleozoic or Precambrian metasedimentary rocks which are are poorly represented by the lithological maps (Stevens and Greene, 1999). $^{87}Sr/^{86}Sr$ signature is also slightly overestimated by our models in streams within the Long Valley caldera such as

Fig. 7. Catchment water model validation results. Modeled and measured $^{87}Sr/^{86}Sr$ in (A and B) 12 streams of the Clarks Fork of the Yellowstone River Basin in Wyoming (Horton et al., 1999); (C and D) 19 streams of the Owen Lake in California (Pretti and Stewart, 2002); (E and F) 19 samples from the Scioto River Basin in Ohio (Stueber et al., 1975); (G and H) 18 streams of the Susquehanna River Basin in Pennsylvannia (Fisher and Stueber, 1976). Black circle: observations; Open circle: age-only water model; Open triangle: unweighted catchment water model; Reversed black triangle: flux weighed catchment water model; Black square: celestite-corrected flux-weighted catchment water model for the Scioto River Basin. Dashed lines in the right hand panels show the 1:1 relationship.

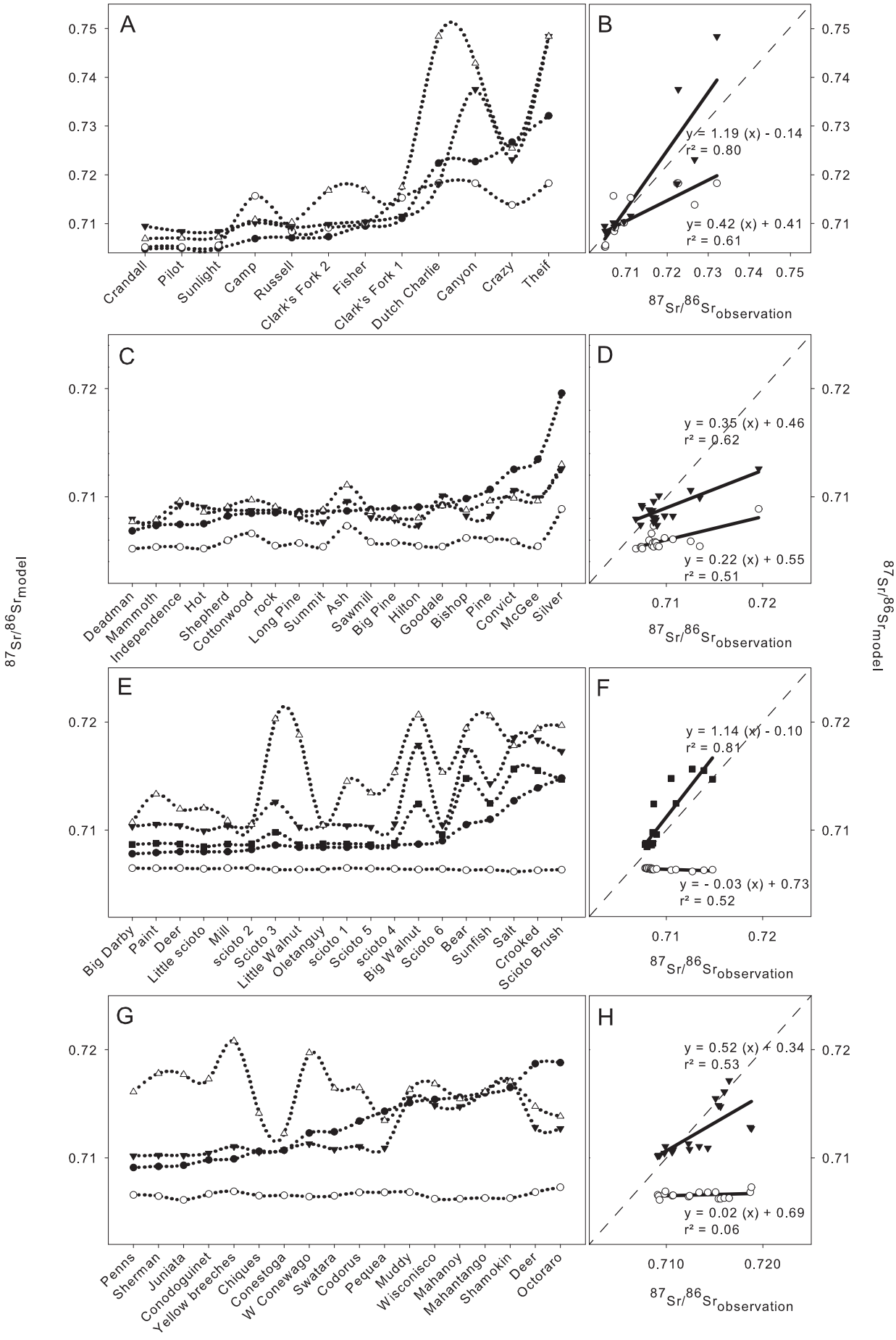
A
B
C
D
E
F
G
H
$^{87}Sr/^{86}Sr_{model}$
$^{87}Sr/^{86}Sr_{observation}$
y = 1.19 (x) - 0.14
r² = 0.80
y= 0.42 (x) + 0.41
r² = 0.61
y = 0.35 (x) + 0.46
r² = 0.62
y = 0.22 (x) + 0.55
r² = 0.51
y = 1.14 (x) - 0.10
r² = 0.81
y = - 0.03 (x) + 0.73
r² = 0.52
y = 0.52 (x) + 0.34
r² = 0.53
y = 0.02 (x) + 0.69
r² = 0.06
Crandall
Pilot
Sunlight
Camp
Russell
Clark's Fork 2
Fisher
Clark's Fork 1
Dutch Charlie
Canyon
Crazy
Theif
Deadman
Mammoth
Independence
Hot
Shepherd
Cottonwood
rock
Long Pine
Summit
Ash
Sawmill
Big Pine
Hilton
Goodale
Bishop
Pine
Convict
McGee
Silver
Big Darby
Paint
Deer
Little scioto
Mill
scioto 2
Scioto 3
Little Walnut
Oletanguy
scioto 1
Scioto 5
scioto 4
Big Walnut
Scioto 6
Bear
Sunfish
Salt
Crooked
Scioto Brush
Penns
Sherman
Juniata
Conodoguinet
Yellow breeches
Chiques
Conestoga
W Conewago
Swatara
Codorus
Pequea
Muddy
Wisconisco
Mahanoy
Mahantango
Shamokin
Deer
Octoraro

Independence and Hot creeks. This area is characterized by low $^{87}Sr/^{86}Sr$ rocks and hydrothermal springs which contribute greatly to the water chemistry (Pretti and Stewart, 2002). Measured $^{87}Sr/^{86}Sr$ values for hot springs of the area ranged from 0.7078 to 0.7081 (Goff et al., 1991) which may explain the discrepancy with our modeled $^{87}Sr/^{86}Sr$. Pretti and Stewart (2002) also showed that these hot springs exert a strong influence at large scale, on the downstream $^{87}Sr/^{86}Sr$ value of the Owens River because of their high dissolved Sr load, an influence that would not be accounted for in our model. Other potential factors explaining the inaccuracy of the models include inputs of Sr from mineral dust (Clow et al., 1997), the poor representation of the geological complexity of these watersheds by 2D maps, or the inaccuracy of our weathering equations when several lithological weathering rates have to be approximated concomitantly.

For the Scioto River Basin, the unweighted catchment water model drastically overestimates the $^{87}Sr/^{86}Sr$ value in stream water in several catchments, whereas the age-only model underestimates the observed values (Fig. 7E). The flux-weighted catchment water model reduces the magnitude of overestimates relative to the unweighted catchment water model for almost all the watersheds, a difference that can be attributed to the higher Sr flux from carbonate units in the watersheds in comparison with silicates (Table 1). Several sub-watersheds in the Southern part of the Basin that are dominated by shales, such as Bear, Salt, Crooked and Scioto Brush Creeks, display low $^{87}Sr/^{86}Sr$ measurements relative to the high $^{87}Sr/^{86}Sr$ of their bedrock. This anomaly is due to the presence of minor amount of calcite in these shales (Table 1), which weathers preferentially and buffers the $^{87}Sr/^{86}Sr$ of the weathering flux. The Sr isotope ratio in two other sub-watersheds (Big Walnut and Scioto 3) with bedrock geology exclusively composed of silicates (Table 1) is overestimated by the flux-weighted catchment water model. However, these sub-watersheds are proximal to outcropping carbonate formations, and drillings from these catchments show that thick layers of carbonates are present at depth (Stueber et al., 1975). Groundwater discharged from these beds probably buffers the $^{87}Sr/^{86}Sr$ and explains the discrepancy between model and measurements (Fig. 7E).

Apart from these specific examples, the catchment water model shows a general tendency to overestimate the $^{87}Sr/^{86}Sr$ of watersheds of this Basin. Stueber et al. (1975) showed that glacial overburden within the Scioto River Basin, which contains a large amount of soluble celestite ($SrSO_4$) and pulverized Paleozoic carbonates with $^{87}Sr/^{86}Sr$ equal to 0.708 (Table 1), buffers the $^{87}Sr/^{86}Sr$ in these streams (Stueber et al., 1975). To attempt to account for this factor, we developed a correction for the contribution of till and carbonates to water. We based this correction on the work of Steele et al. (1972) who used the Sr concentration in water to estimate the contribution of each source of Sr. We used a surficial geology map (Clawges et al., 1999) to identify the distribution of glacial till the Basin. In each subwatershed covered by thick and thin glacial deposits, respectively, we considered that celestite contributed 75% (average contribution for watersheds covered by thick glacial till in Steele et al., 1972) and 50% (average contribution for watersheds covered by thin glacial till in Steele et al., 1972) of the Sr in water. The celestite-corrected water model substantially improved the accuracy of predictions within this Basin, explaining 81% of the variance with a model/data slope close to 1 (Fig. 7E and F). This result suggests that future work should include improved model formulations representing surficial deposits, particularly in area where thick glacial and eolian deposits are present. One impediment to this work is the relatively limited availability of systematic information on the age, origin and composition of these surficial deposits.

For the Susquehanna River Basin, the flux-weighted catchment water model dramatically improves the model predictions relative to the age-only and unweighted catchment water models (Fig. 7G and H). In most of the watersheds, the unweighted catchment water model overestimates the $^{87}Sr/^{86}Sr$ whereas the flux-weighted catchment water model matches the observations closely because of the importance given to preferential dissolution of carbonates. The improved performance of the flux-weighted catchment water model is seen here despite the divergence between bedrock model predictions and measurements for shales (Table 1). Similar to the Scioto Basin, shale leachates here have a significantly lower $^{87}Sr/^{86}Sr$ than the whole rock due to the selected dissolution of minor amount of calcite (Table 1). The discrepancy between the flux-weighted catchment water model and observed $^{87}Sr/^{86}Sr$ values for Deer and Octoraro creeks can be explained by the inability of the bedrock model to accurately predict the $^{87}Sr/^{86}Sr$ of rocks from the Wissahickon Formation (Table 1).

4.2.2. A global view of the catchment water model

The flux-weighted catchment water model explains 70% of the variance of the Sr isotopes in water for the 68 watersheds tested with a linear correlation close to the 1:1 relationship (Fig. 8). Prediction accuracy for this model, estimated based on the validation data, is significantly improved relative to the other models, with MAE = 0.00051 and RMSE = 0.0034. In comparison, the age-only catchment water model explains 38% of the observed variance with MAE = −0.0039 and RMSE = 0.0056. In our approach, we added a number of lithological effects that increased the accuracy of water $^{87}Sr/^{86}Sr$ predictions in most of the geological settings. The resulting local water (Fig. 9A) and flux-weighted catchment water (Fig. 9B) maps for the contiguous USA show patterned $^{87}Sr/^{86}Sr$ variations similar to the bedrock models (Fig. 6A and B). Average $^{87}Sr/^{86}Sr$ values are highest in the new bedrock model and lowest in the flux-weighted catchment water model, where the preferential dissolution of low $^{87}Sr/^{86}Sr$ units (e.g. carbonates and mafic rocks) buffers the $^{87}Sr/^{86}Sr$ of the water catchment model in comparison with bedrock (Fig. 6D).

The maps predict large variations at a range of spatial resolutions, which are promising for provenance studies. Nevertheless, the $^{87}Sr/^{86}Sr$ prediction in water could be improved by considering the potential contribution of non-bedrock sources of Sr to water (Sillen et al., 1998; Stewart et al., 1998). In our validation process, we demonstrated the importance of accounting for the contribution of Sr-rich minerals (calcite, dolomite and celestite) because they often buffer the $^{87}Sr/^{86}Sr$ of whole rivers. Similarly, the effect of dust deposition in the Rockies (Clow et al., 1997), contributions from soil and surficial materials (Stewart et al., 1998) and the effect of local phenomenon such as hydrothermal contributions (Pretti and Stewart, 2002) and atmospheric deposition (Stewart et al., 1998) should be considered in future work.

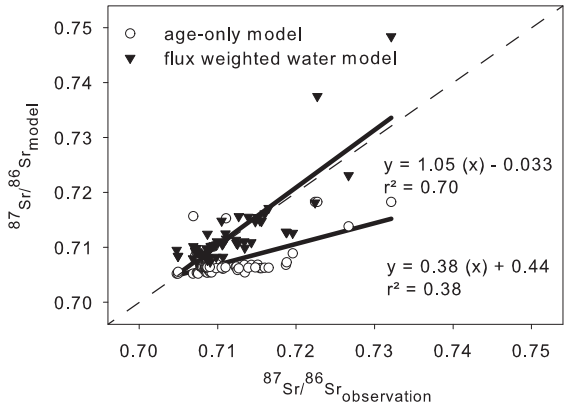

Fig. 8. Validation of the catchment water Sr isotope model across all study catchments, showing linear regressions between measured $^{87}Sr/^{86}Sr$ and flux-weighted catchment water and age-only water model predictions for 68 streams of the USA (celestite-corrected values are used for the Scioto River). Dashed line shows the 1:1 relationship.

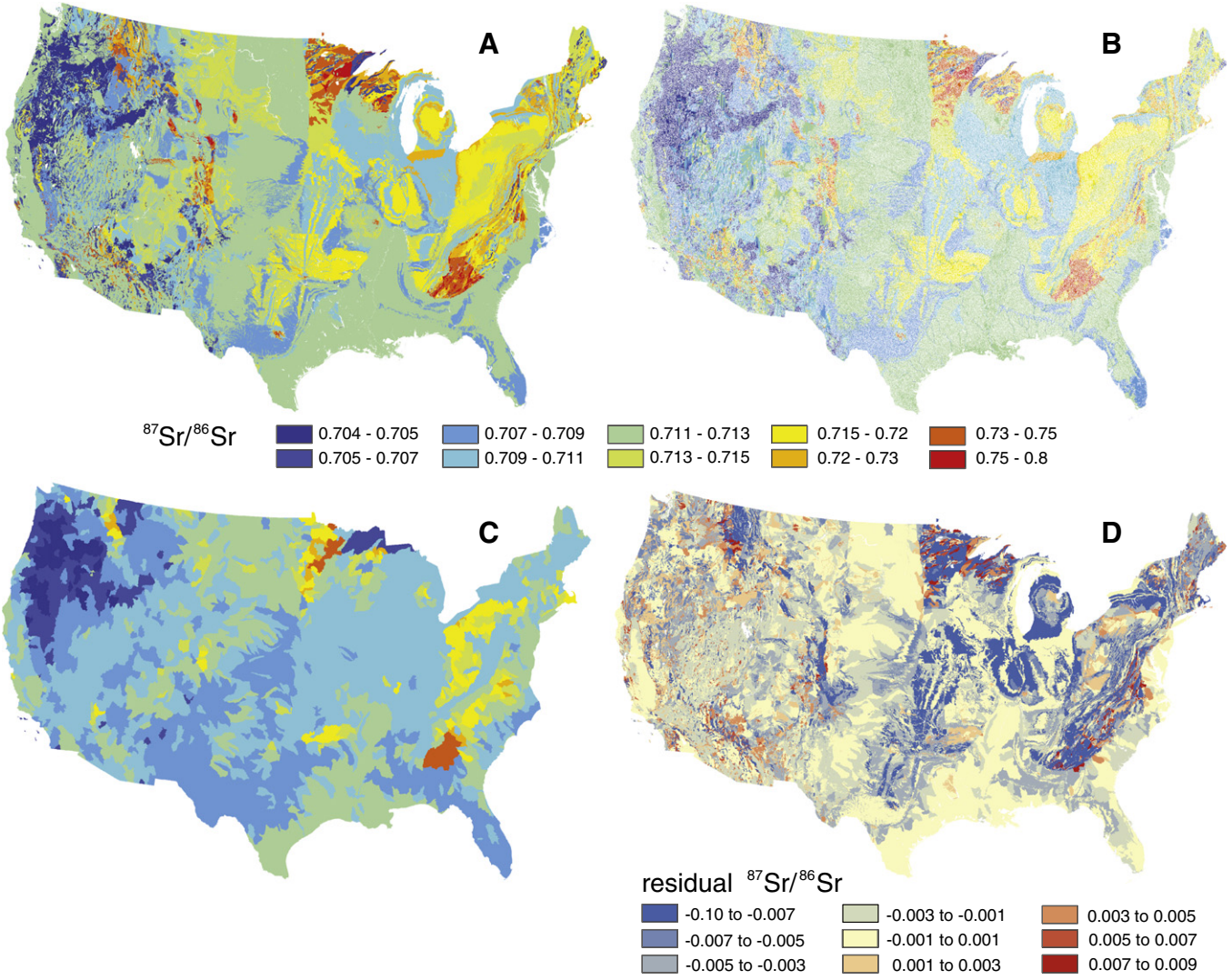

Fig. 9. Modeled Sr isotope ratios for (A) local water, (B) flux-weighted catchment water, (C) flux-weighted catchment water model values averaged within watersheds of the Watershed Boundary Dataset (http://www.nrcs.usda.gov/wps/portal/nrcs/main/national/water/watersheds/dataset) and (D) residual between major bedrock (Fig. 6B) and average flux-weighted catchment water (Fig. 9C).

Applying predictive models to interpret the $^{87}Sr/^{86}Sr$ of biological materials is challenging because the contribution of different environmental sources of Sr to the organism are often unknown. In this study, we consider bedrock and water as two potential sources of Sr to plants, and compare our model predictions with data on the $^{87}Sr/^{86}Sr$ of marijuana measured for forensic purposes (West et al., 2009). Comparisons with this dataset were based on model values integrated across counties, as this was the most precise level of geographic information reported for the marijuana samples.

The flux-weighted catchment water model showed the strongest correlation and most accurate predictions in comparison with the measured marijuana sample $^{87}Sr/^{86}Sr$ values (Fig. 10). In contrast, the unweighted catchment water model showed the weakest correlation with the measured values. The strength of correlation for the age-only water model was intermediate, but this model drastically under-predicted the range of observed values (Fig. 10). $^{87}Sr/^{86}Sr$ predictions for several counties are buffered by the presence of carbonate bedrock, which explains the differences between the unweighted and flux-weighted catchment water models and supports the hypothesis of West et al. (2009) that carbonate bedrock effects were reflected in the marijuana Sr isotope dataset. Most of the marijuana $^{87}Sr/^{86}Sr$ values were approximated well by the flux-weighted catchment water model, however significant inaccuracies remain in complex geological settings such as on the Minnesota shield or in the Appalachian Mountains. The correlations observed for the different models suggest that the $^{87}Sr/^{86}Sr$ value in plants is closer to a flux-weighted $^{87}Sr/^{86}Sr$ signal integrated over a large area (flux-weighted catchment water model) than to an unweighted average of the soluble $^{87}Sr/^{86}Sr$ of the rock units of the county (unweighted catchment water model). Although these results offer no direct information on the ultimate sources of Sr to marijuana plants, they suggest that spatial model formulations that more accurately represent bedrock Sr isotope ratios and account for weathering effects on Sr release to water may more accurately represent the isotope ratios of Sr taken up by these plants. Integrating the $^{87}Sr/^{86}Sr$ values over a county area likely reduces the accuracy of these comparisons given that these political boundaries usually do not have any significance in terms of hydrology, and this methodological issue could also help explain the weak correlation of the unweighted catchment water model in comparison with the age-only catchment model.

5. Conclusion and perspectives

We have developed and calibrated parameterized models for the prediction of regional to continental scale spatial variation in bedrock and catchment water Sr isotope ratios. Unlike previous models, our

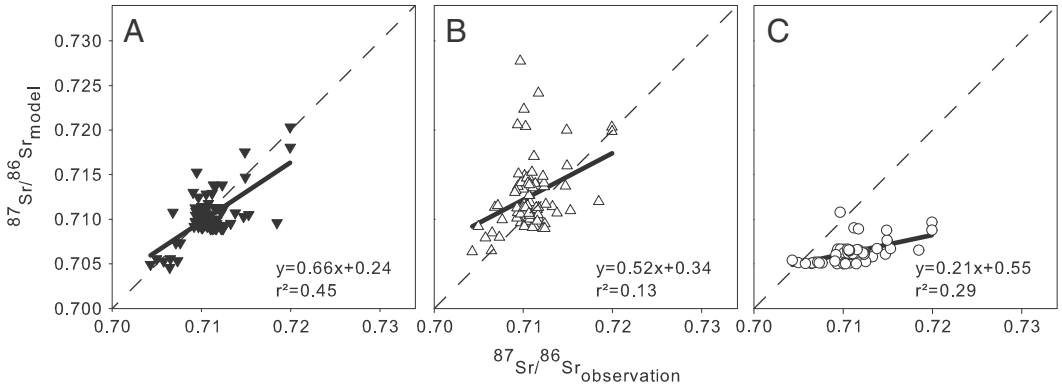

Fig. 10. Linear regression between $^{87}Sr/^{86}Sr$ in marijuana and the mean values of the modeled water in the county of sample origin. Water values are the average of all grid cells in the county, weighted as described for the (A) flux-weighted catchment water model, (B) unweighted catchment water model, and (C) age-only catchment water model. Symbols as in Fig. 7. Dashed line in each panel shows the 1:1 relationship.

formulation represents major lithology-specific effects and yet remains generalized to the extent that it could be applied in any region where basic digital geological map data (including lithology and age) are available. In spite of the limitations discussed throughout this paper, this new mapping method represents a significant advance in modeling major environmental Sr sources to ecosystems, and the strength of the correlations between the different models and the observations are encouraging. Moreover, although the predictive power of the model remains limited in many cases, our documentation of model performance through quantitative comparisons with observational data allows informed use of the model-derived data products.

A number of regions of the contiguous USA display promising $^{87}Sr/^{86}Sr$ variations at different scales which could be used to determine rock, water or biological material provenance. The Sr isoscapes could complement other existing isoscapes (Bowen et al., 2005) used for provenance studies because $^{87}Sr/^{86}Sr$ varies widely at regional and continental scales. The development of more detailed and harmonized seamless geological maps for the conterminous USA (Jansen et al., 2010) and other regions, as well as refined high resolution lithological studies and geochemical sampling, could rapidly improve the resolution and accuracy of these isoscapes.

In this respect, we suggest the following as critical next steps to improving the predictability of environmental Sr isotope ratios at large scales:

1) Develop more flexible parameterizations and parameter distributions that increase the ability of the model to represent highly radiogenic rock units.
2) Improve weathering rate calculations by including functions describing rate dependence on factors such as runoff, climate, pedology, vegetation and topography. Recent work from Jansen et al. (2010) offers a good starting point.
3) Develop submodels representing the contribution of atmospheric sources of Sr, particularly dust and sea salt, to soil and bioavailable Sr.
4) Identify systematic approaches to representing the contribution of Sr weathered from surficial deposits to water.
5) Ultimately, model and scale the contribution of these sources of Sr, including bedrock weathering, atmospheric sources and surficial Sr sources, to bioavailable and biological pools of interest, including soil, soil water, surface and groundwater and organismal Sr. The work of Stewart et al. (1998) provides a platform on which such an effort could be developed.
6) In all cases, these efforts will be advanced through the continued accumulation and compilation of Sr isotope measurements and elemental concentration data from a range of materials. Our results suggest that the most critical data gaps vary depending on location, but include measurements of surficial deposits that are not adequately characterized on most geological maps and continued analysis of Sr isotope ratios of stream systems, which integrate the geochemistry of their watersheds and can reveal important inaccuracies in the model.

Acknowledgements

This research was supported by NSF Award DBI-0743543. We thank Casey Kennedy and Hilary Bataille for reviewing and commenting on this manuscript, and three anonymous reviewers for their comments which greatly improved this manuscript.

Appendix A. Supplementary data

Supplementary data to this article can be found online at doi:10.1016/j.chemgeo.2012.01.028.

References

Anderson, S.P., Drever, J.I., Frost, C.D., Holden, P., 2000. Chemical weathering in the foreland of a retreating glacier. Geochimica et Cosmochimica Acta 64 (7), 1173–1189.
Barnett-Johnson, R., Pearson, T.E., Ramos, F.C., Grimes, C.B., MacFarlane, R.B., 2008. Tracking natal origins of salmon using isotopes, otoliths, and landscape geology. Limnology and Oceanography 53 (4), 1633–1642.
Beard, B.L., Johnson, C.M., 2000. Strontium isotope composition of skeletal material can determine the birth place and geographic mobility of humans and animals. Journal of Forensic Sciences 45 (5), 1049–1061.
Bentley, R.A., 2006. Strontium isotopes from the earth to the archaeological skeleton: a review. Journal of Archaeological Method and Theory 13 (3), 135–187. doi:10.1007/s10816-006-9009-x.
Bentley, R.A., Knipper, C., 2005. Geographical patterns in biologically available strontium, carbon and oxygen isotope signatures in prehistoric SW Germany. Archaeometry 47, 629–644.
Bentley, R.A., Wahl, J., Price, T.D., Atkinson, T.C., 2008. Isotopic signatures and hereditary traits: snapshot of a Neolithic community in Germany. Antiquity 82 (316), 290–304.
Beusen, A.H.W., Bouwman, A.F., Durr, H.H., Dekkers, A.L.M., Hartmann, J., 2009. Global patterns of dissolved silica export to the coastal zone: results from a spatially explicit global model. Global Biogeochemical Cycles 23.
Bluth, G.J.S., Kump, L.R., 1994. Lithologic and climatologic controls of river chemistry. Geochimica et Cosmochimica Acta 58 (10), 2341–2359.
Bowen, G.J., 2010. Isoscapes: spatial pattern in isotopic biogeochemistry. Annual Review of Earth and Planetary Sciences 38, 161–187. doi:10.1146/annurev-earth-040809-152429.
Bowen, G.J., Wassenaar, L.I., Hobson, K.A., 2005. Global application of stable hydrogen and oxygen isotopes to wildlife forensics. Oecologia 143 (3), 337–348. doi:10.1007/s00442-004-1813-y.
Brady, P.V., Carroll, S.A., 1994. Direct effects of CO2 and temperature on silicate weathering — possible implications for climate control. Geochimica et Cosmochimica Acta 58 (7), 1853–1856.
Brantley, S.L., Goldhaber, M.B., Ragnarsdottir, K.V., 2007. Crossing disciplines and scales to understand the Critical Zone. Elements 3 (5), 307–314.

Bullen, T.D., Krabbenhoft, D.P., Kendall, C., 1996. Kinetic and mineralogic controls on the evolution of groundwater chemistry and 87Sr/86Sr in a sandy silicate aquifer, northern Wisconsin, USA. Geochimica et Cosmochimica Acta 60 (10), 1807–1821.

Capo, R.C., Stewart, B.W., Chadwick, O.A., 1998. Strontium isotopes as tracers of ecosystem processes: theory and methods. Geoderma 82 (1–3), 197–225.

Carlson, R.W., 2003. Introduction to Volume 2. In: Heinrich, D.H., Karl, K.T. (Eds.), Treatise on Geochemistry. Pergamon, Oxford, pp. xv–xxiii.

Chadwick, O.A., Derry, L.A., Bern, C., 2009. Changing sources of strontium to soils and ecosystems across the Hawaiian Islands. Chemical Geology 267, 64–76. doi:10.1016/j.chemgeo.2009.01.009.

Chamberlain, C.P., et al., 1997. The use of isotope tracers for identifying populations of migratory birds. Oecologia 109 (1), 132–141.

Chaudhuri, S., Clauer, N., 1993. Strontium isotopic compositions and potassium and rubidium contents of formation waters in sedimentary basins — clues to the origin of the solutes. Geochimica et Cosmochimica Acta 57 (2), 429–437.

Clawges, R.M., Price, C.V., National Water-Quality Assessment Program (U.S.) and Geological Survey (U.S), 1999. Digital data sets describing principal aquifers, surficial geology, and ground-water regions of the conterminous United States. U S Geological Survey open-file report 99–77. USGS, Rapid City, S.D.

Clow, D.W., Mast, M.A., Bullen, T.D., Turk, J.T., 1997. Strontium 87 strontium 86 as a tracer of mineral weathering reactions and calcium sources in an alpine/subalpine watershed, Loch Vale, Colorado. Water Resources Research 33 (6), 1335–1351.

Crittenden, R.G., et al., 2007. Determining the geographic origin of milk in Australasia using multi-element stable isotope ratio analysis. International Dairy Journal 17 (5), 421–428. doi:10.1016/j.idairyj.2006.05.012.

Dasch, E.J., 1969. Strontium isotopes in weathering profiles, deep-sea sediments, and sedimentary rocks. Geochimica et Cosmochimica Acta 33 (12) 1521–&.

Davies, G.R., Halliday, A.N., 1998. Development of the Long Valley rhyolitic magma system: strontium and neodymium isotope evidence from glasses and individual phenocrysts. Geochimica et Cosmochimica Acta 62 (21–22), 3561–3574.

DePaolo, D.J., 1981. Trace element and isotopic effects of combined wallrock assimilation and fractional crystallization. Earth and Planetary Science Letters 53 (2), 189–202. doi:10.1016/0012-821x(81)90153-9.

Drever, J.I., Clow, D.W., 1995. Weathering rates in catchments. In: Brantley, S., White, A. (Eds.), Chemical weathering rates of silicate minerals. : Rev. in Mineral., vol. 31. Mineral. Soc. of Am., Washington, D. C., pp. 463–483.

Eckhardt, F.E.W., 1979. Über die Einwirkung heterotropher Mikroorganismen auf die Zersetzung silikatischer Minerale. Zeitschrift für Pflanzenernährung und Bodenkunde 142 (3), 434–445.

Ezzo, J.A., Johnson, C.M., Price, T.D., 1997. Analytical perspectives on prehistoric migration: a case study from east-central Arizona. Journal of Archaeological Science 24 (5), 447–466.

Faure, G., 1977. Principles of isotope geology. Related Information: Smith and Wyllie intermediate geology series. Medium: X; Size: Pages: 475 pp.

Fisher, R.S., Stueber, A.M., 1976. Strontium isotopes in selected streams within Susquehanna River Basin. Water Resources Research 12 (5), 1061–1068.

Franke, W.A., 2009. The durability of rocks — developing a test of rock resistance to chemical weathering. American Journal of Science 309 (8), 711–730. doi:10.2475/08.2009.04.

Frei, R., Frei, K.M., 2011. The geographic distribution of strontium isotopes in Danish surface waters — a base for provenance studies in archaeology, hydrology and agriculture. Applied Geochemistry 26, 326–340.

Geological Survey (U.S.), 2004. The National Geochemical Survey, database and documentation, U S Geological Survey open-file report 2004-1001. U.S. Dept. of the Interior, U.S. Geological Survey, [Reston, Va.].

Geological Survey (U.S), 2005. State Geologic Map Compilation, U S Geological Survey open-file report (various), online at http://tin.er.usgs.gov/geology/state/.

Geological Survey (U.S.). Geologic Names Committee, 2007. Divisions of geologic time — major chronostratigraphic and geochronologic units. Fact sheet 2007–3015. U.S. Geological Survey, [Reston, Va.].

Gesch, D., 2002. The National Elevation Dataset. Photogrammetric Engineering and Remote Sensing 68 (1) 5–+.

Goff, F., Wollenberg, H.A., Brookins, D.C., Kistler, R.W., 1991. A Sr-isotopic comparison between thermal waters, rocks, and hydrothermal calcites, Long Valley Caldera, California. Journal of Volcanology and Geothermal Research 48 (3–4), 265–281.

Goldstein, S.J., Jacobsen, S.B., 1988. Nd and Sr isotopic systematics of river water suspended material — implications for crustal evolution. Earth and Planetary Science Letters 87 (3), 249–265.

Graustein, W.C., 1989. $^{87}Sr/^{86}Sr$ ratios measure the sources and flow of strontium in terrestrial ecosystems. Stable isotopes in ecological research. Ecological Studies 68, 491–512.

Graustein, W.C., Armstrong, R.L., 1983. The use of Sr-87 Sr-86 ratios to measure atmospheric transport into forested watersheds. Science 219 (4582), 289–292.

Grousset, F.E., Biscaye, P.E., 2005. Continental aerosols, isotopic fingerprints of sources and atmospheric transport: a review. Chemical Geology 222, 149–167.

Hartmann, J., Moosdorf, N., 2011. Chemical weathering rates of silicate-dominated lithological classes and associated liberation rates of phosphorus on the Japanese Archipelago — implications for global scale analysis. Chemical Geology. doi:10.1016/j.chemgeo.2010.12.004.

Hartmann, J., Jansen, N., Dürr, H.H., Harashima, A., Okubo, K., Kempe, S., 2009. Predicting riverine dissolved silica fluxes into coastal zones from a hyperactive region and analysis of their first order controls. International Journal of Earth Sciences. doi:10.1007/s00531-008-0381-5.

Hodell, D.A., Quinn, R.L., Brenner, M., Kamenov, G., 2004. Spatial variation of strontium isotopes (Sr-87/Sr-86) in the Maya region: a tool for tracking ancient human migration. Journal of Archaeological Science 31 (5), 585–601. doi:10.1016/j.jas.2003.10.009.

Hogan, J.F., Blum, J.D., Siegel, D.I., Glaser, P.H., 2000. Sr-87/Sr-86 as a tracer of groundwater discharge and precipitation recharge in the Glacial Lake Agassiz Peatlands, northern Minnesota. Water Resources Research 36 (12), 3701–3710.

Hoppe, K.A., Koch, P.L., Carlson, R.W., Webb, S.D., 1999. Tracking mammoths and mastodons: reconstruction of migratory behavior using strontium isotope ratios. Geology 27 (5), 439–442.

Horton, T.W., Chamberlain, C.P., Fantle, M., Blum, J.D., 1999. Chemical weathering and lithologic controls of water chemistry in a high-elevation river system: Clark's Fork of the Yellowstone River, Wyoming and Montana. Water Resources Research 35 (5), 1643–1655.

Jansen, N., Hartmann, J., Lauerwald, R., Dürr, H.H., Kempe, S., Loos, S., Middelkoop, H., 2010. Dissolved silica mobilization in the conterminous USA. Chemical Geology 270 (1–4), 90–109. doi:10.1016/j.chemgeo.2009.11.008.

Kawasaki, A., Oda, H., Hirata, T., 2002. Determination of strontium isotope ratio of brown rice for estimating its provenance. Soil Science and Plant Nutrition 48 (5), 635–640.

Kelly, S., Heaton, K., Hoogewerff, J., 2005. Tracing the geographical origin of food: the application of multi-element and multi-isotope analysis. Trends in Food Science & Technology 16 (12), 555–567. doi:10.1016/j.tifs.2005.08.008.

King, E.M., Beard, B.L., Valley, J.W., 2007. Strontium and oxygen isotopic evidence for strike/slip movement of accreted terranes in the Idaho Batholith. Lithos 96, 387–401.

Kistler, R.W., Peterman, Z.E., 1973. Variations in Sr, Rb, K, Na, and initial Sr-87–Sr-86 in Mesozoic granitic rocks and intruded wall rocks in Central California. Geological Society of America Bulletin 84 (11), 3489–3511.

Koch, P.L., et al., 1995. Isotopic tracking of change in diet and habitat use in African elephants. Science 267 (5202), 1340–1343.

Le Bas, M.J., Streckeisen, A.L., 1991. The IUGS systematics of igneous rocks. Journal of the Geological Society 148 (5), 825–833. doi:10.1144/gsjgs.148.5.0825.

Lehnert, K., Su, Y., Langmuir, C.H., Sarbas, B., Nohl, U., 2000. A global geochemical database structure for rocks. Geochemistry, Geophysics, Geosystems 1 (5), 1–14. doi:10.1029/1999gc000026.

Lewis, M.A., 1989. Water. In: McCall, J., Marker, B. (Eds.), Earth Science Mapping for planning, development and conservation. Graham and Trotman.

Marchand, D.E., 1974. Chemical weathering, soil development, and geochemical fractionation in a part of the White Mountains, Mono and Inyo Counties, California. Geological Survey Professional Paper 352-J: Erosion and Sedimentation in a Semi-arid Environment. U.S. Govt. Print. Off, Washington, pp. 379–424. v p.

Matsukura, Y., Hattanji, T., Oguchi, C.T., Hirose, T., 2007. Ten year measurements of weathering rates of rock tablets on a forested hillslope in a humid temperate region, Japan. Zeitschrift Fur Geomorphologie 51 (1), 27–40. doi:10.1127/0372-8854/2007/0051s-0027.

Meybeck, M., 1987. Global chemical weathering of surficial rocks estimated from river dissolved loads. American Journal of Science 287 (5), 401–428.

Miller, E.K., Blum, J.D., Friedland, A.J., 1993. Determination of soil exchangeable-cation loss and weathering rates using Sr isotopes. Nature 362 (6419), 438–441.

Moulton, K.L., West, J., Berner, R.A., 2000. Solute flux and mineral mass balance approaches to the quantification of plant effects on silicate weathering. American Journal of Science 300 (7), 539–570.

Négrel, Ph., Petelet-Giraud, E., 2005. Strontium isotopes as tracers of groundwater-induced floods: the Somme case study (France). Journal of Hydrology 305, 99–119.

Pretti, V.A., Stewart, B.W., 2002. Solute sources and chemical weathering in the Owens Lake watershed, eastern California. Water Resources Research 38 (8) doi:Artn 1127.

Price, T.D., Johnson, C.M., Ezzo, J.A., Ericson, J., Burton, J.H., 1994. Residential-mobility in the prehistoric Southwest United-States — a preliminary-study using strontium isotope analysis. Journal of Archaeological Science 21 (3), 315–330.

Price, T.D., Burton, J.H., Bentley, R.A., 2002. The characterization of biologically available strontium isotope ratios for the study of prehistoric migration. Archaeometry 44, 117–136.

Raymo, M.E., Ruddiman, W.F., Froelich, P.N., 1988. Influence of late Cenozoic mountain building on ocean geochemical cycles. Geology 16 (7), 649–653.

Reimann, C., Filzmoser, P., 2000. Normal and lognormal data distribution in geochemistry: death of a myth. Consequences for the statistical treatment of geochemical and environmental data. Environmental Geology 39, 1001–1014.

Rudnick, R.L., 2003. Introduction to Volume 3. In: Heinrich, D.H., Karl, K.T. (Eds.), Treatise on Geochemistry. Pergamon, Oxford, pp. xv–xix.

Shields, G., Veizer, J., 2002. Precambrian marine carbonate isotope database: Version 1.1. Geochemistry, Geophysics, Geosystems 3 doi:Artn 1031.

Sillen, A., Hall, G., Richardson, S., Armstrong, R., 1998. 87Sr/86Sr ratios in modern and fossil food-webs of the Sterkfontein Valley: implications for early hominid habitat preference. Geochimica et Cosmochimica Acta 62 (14), 2463–2473. doi:10.1016/s0016-7037(98)00182-3.

Steele, J.D., Stueber, A.M., Curtis, J.B., Pushkar, P., 1972. Strontium isotopic study of Scioto River Basin, Ohio. Transactions — American Geophysical Union 53 (4) 379–&.

Stevens, C.H., Greene, D.C., 1999. Stratigraphy, depositional history, and tectonic evolution of Paleozoic continental-margin rocks in roof pendants of the eastern Sierra Nevada, California. Geological Society of America Bulletin 111, 919–933.

Stewart, B.W., Capo, R.C., Chadwick, O.A., 1998. Quantitative strontium isotope models for weathering, pedogenesis and biogeochemical cycling. Geoderma 82 (1–3), 173–195.

Stueber, A.M., Baldwin, A.D., Curtis, J.B., Pushkar, P., Steele, J.D., 1975. Geochemistry of strontium in Scioto River Drainage Basin, Ohio. Geological Society of America Bulletin 86 (7), 892–896.

Veizer, J., et al., 1999. Sr-87/Sr-86, delta C-13 and delta O-18 evolution of Phanerozoic seawater. Chemical Geology 161 (1–3), 59–88.

Voerkelius, S., et al., 2010. Strontium isotopic signatures of natural mineral waters, the reference to a simple geological map and its potential for authentication of food. Food Chemistry 118 (4), 933–940. doi:10.1016/j.foodchem.2009.04.125.

Wasserbu, G.J., Papanast, D.A., Sanz, H.G., 1969. Initial strontium for a chondrite and determination of a metamorphism or formation interval. Earth and Planetary Science Letters 7 (1) 33–&.
West, A.J., Galy, A., Bickle, M., 2005. Tectonic and climatic controls on silicate weathering. Earth and Planetary Science Letters 235 (1–2), 211–228.
West, J.B., Hurley, J.M., Dudas, F.O., Ehleringer, J.R., 2009. the stable isotope ratios of Marijuana. II. Strontium isotopes relate to geographic origin. Journal of Forensic Sciences 54 (6), 1261–1269. doi:10.1111/j.1556-4029.2009.01171.x.
Wetheril, G.W., Davis, G.L., Leehu, C., 1968. Rb–Sr measurements on whole rocks and separated minerals from Baltimore Gneiss Maryland. Geological Society of America Bulletin 79 (6) 757–&.
White, A.F., Blum, A.E., 1995. Effects of climate on chemical-weathering in watersheds. Geochimica et Cosmochimica Acta 59 (9), 1729–1747.
Whitney, P.R., Hurley, P.M., 1964. The problem of inherited radiogenic strontium in sedimentary age determinations. Geochimica et Cosmochimica Acta 28, 425–436 (Apr).